INTERNATIONAL JOURNAL OF CONSERVATION SCIENCE

ISSN: 2067-533X Volume 8, Issue 4, October-December 2017: 675-684 www.ijcs.uaic.ro

X-RAY PHOTOELECTRON SPECTROSCOY IN THE STUDY OF THE CHEMISTRY OF A DAGUERREOTYPE SURFACE

Madalena S. KOZACHUK[1*], Tsun-Kong SHAM[1*], Ronald R. MARTIN[1], Mike ROBINSON[2], Andrew J. NELSON[3], Mark C. BIESINGER[4]

[1] *The University of Western Ontario, The Department of Chemistry, 1151 Richmond Street, London, Ontario, N6A 5B7, Canada*
[2] *Century Darkroom, 245 Carlaw Avenue, Studio 502, Toronto, Ontario, M4M 2S1, Canada*
[3] *The University of Western Ontario, The Department of Anthropology, 1151 Richmond Street, London, Ontario, N6A 3A2, Canada*
[4] *The University of Western Ontario, Surface Science Western, 999 Collip Circle, P.O. Box 12, London, Ontario, N6G 0J3, Canada*

Abstract

Laboratory and synchrotron-based X-ray Photoelectron Spectroscopy (XPS) were used to study the element distribution and chemistry of a specially prepared daguerreotype plate. The goal of this work was to achieve a greater understanding of how the chemistry of the daguerreian plate changes from surface to subsurface. A silver-gold alloy was expected to vary between highlight and shadow regions. Depth analysis showed that residual halogens and mercury were present on the surface as well as the formation of a silver-gold alloy that varied with depth. Valence band examination indicates minimal alloying between silver, gold, and mercury.

Keywords*: Daguerreotypes; X-ray photoelectron spectroscopy; Scanning electron microscopy; Depth profiling; Synchrotron*

Introduction

In 1839, Louis-Jacques-Mandé Daguerre presented his invention, the daguerreotype, to the members of the French Académie des Sciences [1]. Daguerre's original methodology involved 1) light-sensitizing a highly polished silver surface with an iodide vapour, 2) exposing the plate to light, which induced the photolysis of the silver halide to produce latent image silver particles, 3) developing the plate with mercury vapour, and 4) the removal of excess silver halides with a thiosulfate wash. Later modifications included other halide vapours to increase photosensitivity and gilding with a gold-chloride-thiosulfate solution to improve image contrast [1, 2].

There are many components to the chemical process by which daguerreotype images are produced, many of which have yet to be resolved. Regions that were subjected to bright exposure (i.e., highlight regions) showed image particles of relatively uniform structure and density. Portions of the plate that received little to no exposure (i.e. shadow and dark regions) exhibited image particles with variable size, shape and surface density [3]. The density and size

* Corresponding author: mkozachu@uwo.ca; tsham@uwo.ca

distribution produce a wide variety of gray tones that typify daguerreotypes [4]. While the gilding process provides an even exposure of gold across the entire plate [5], research has shown enhanced gold signal in regions of high image particle density while shadow regions have been observed to contain lower amounts of gold [6, 7], a result of the differing diffusion constants of gold and silver [8]. This simultaneous diffusion of gold into silver and silver into gold produces a silver-gold alloy that varies with depth [6]. The goal of this research is to better understand the physical consequences of this alloy formation, as it is important for the conservation, preservation, storage, and display of these artifacts.

The research undertaken here used synchrotron base high-energy and laboratory-based X-ray photoelectron spectroscopy (HE-XPS and XPS, respectively) in an effort to examine the silver-gold alloy on the surface and the near surface regions beyond 10 nm. The surface sensitivity of lab XPS is well suited to the study of the daguerreotype surface as the detected photoelectrons provide quantitative chemical information and the oxidation states of the elements under study. HE-XPS with high-energy X-rays probe an order of magnitude deeper under the surface, not achievable by lab XPS without destructive ion sputtering. Chemical distribution and speciation with depth was also examined. HE-XPS generates depth information by increasing the energy of the X-ray, which in turn increases the kinetic energy of the photoelectrons hence their escape depth; at a fixed X-ray energy, laboratory-based XPS can provide depth information by surface ablation using ion sputtering techniques. Scanning electron microscopy (SEM) provided microstructure information of select areas.

Materials and Methods

The reference daguerreotype (5□1cm) used in this work (Fig 1) was prepared at Century Darkroom, Toronto (Daguerreotypist, Mike Robinson) using the process described by Humphrey [5] and was used as received. This single plate was analyzed by both the laboratory- and high energy synchrotron-sourced X-rays, labelled XPS and HE-XPS, respectively. Areas for analysis were selected to represent various tones of the image and hence expected to display different surface characteristics.

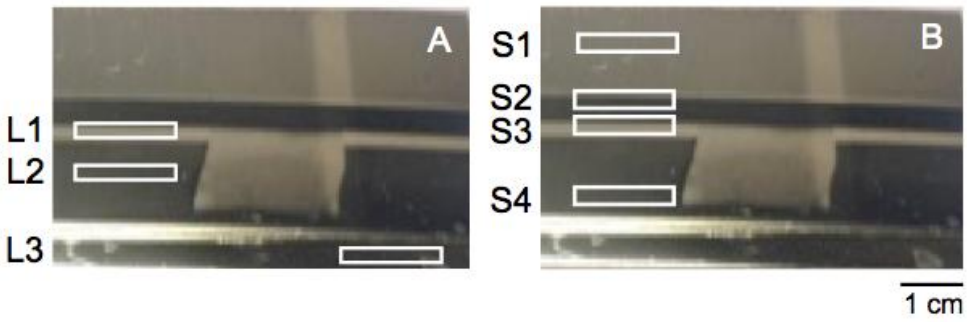

Fig 1. Regions studies on the daguerreotype plate: (A) laboratory-based X-ray photoelectron spectroscopy (L1 - bright, L2 - medium, L3 - dark) and (B) synchrotron-based X-ray photoelectron spectroscopy (S1 - bright medium, S2 - dark, S3 - bright, and S4 -medium). Image taken with a single reflex camera

The laboratory XPS analysis was carried out at Surface Science Western, University of Western Ontario, using a Kratos AXIS Ultra XPS and a monochromatic Al K_α X-ray (1486.7eV, 15mA, 14kV, 210W) with a peak resolution of 0.47eV (Ag $3d_{5/2}$). Instrument base pressure was 1.5 - 2×10^{-9} torr. Fine spectra, including Auger emissions, were collected from all areas. Survey scan and high resolution spectra were acquired from 400 x 400 micron spots using 160eV and 20eV pass energies, respectively. CasaXPS version (2.3.14), XPSPeak, and

Vision 2 Processing Software was used for data processing [9]. Depth profiles were collected using ion ablation to remove sequential surface layers at each region over a period of 41 minutes for L1 and 35 minutes for L2 and L3. A 4kV (15mA) Ar^+ ion beam rastered over an area of 3×3 mm was used for the depth profiling. The sputter rate was estimated to be 1.8nm/min based on an Al_2O_3/Al standard. Due to the varying density of between the Al_2O_3/Al standard and the Ag daguerreian plate, the presented depth profiles for Ag represent an upper bound depth reached as the calculation is based on a relatively less dense, and lighter metal.

The SXRMB (06B1-1) beamline at the Canadian Light Source (CLS) was used for the HE-XPS experiments [10]. Two different excitation energies were used to examine two different depths of the daguerreotype: 3.0keV and 8.0keV; these energies lead to a probing depth of Au 4f of ~10 to ~ 20nm, respectively, based on the density of pure Ag, which is the primary material in the plate. The beam was monochromatized by a Si(111) crystal monochromator. The size of the beam on the sample was 4×1mm in both measurements. A base vacuum of 3.2×10^{-10} torr was maintained. A step size of 400meV was used for survey scans and a step size of 40meV for fine scans. The valence band was collected with a step size of 100meV. The overall energy resolution is ~ 0.6eV at 3000eV and ~ 0.9eV at 8000eV. The IGOR software package (version 6.11) was used to process the collected HE-XPS data [11].

The scanning electron microscopy (SEM) images of the studied regions on the daguerreotype test plate were obtained using the LEO (Zeiss) 1540XB FIB/SEM instrument at the Western Nanofabrication facility. Topographic imaging was performed at 1kV with a working distance (WD) of 4mm and backscatter imaging at 10kV and 9mm.

Results and Discussion

XPS depth profile results

For sample L1, in (Fig 2) suggests that the adventitious carbon signal falls rapidly to a low value around 1.8nm, after which it rises to a somewhat higher value around 3.6nm. Subsequently, the carbon signals then falls to near zero at a depth of 16nm. The rise around 3.6nm corresponds to a small drop in the silver observed in this location. The result may be consistent with the presence of residual carbon black powder from the polishing step during the test plate's production.

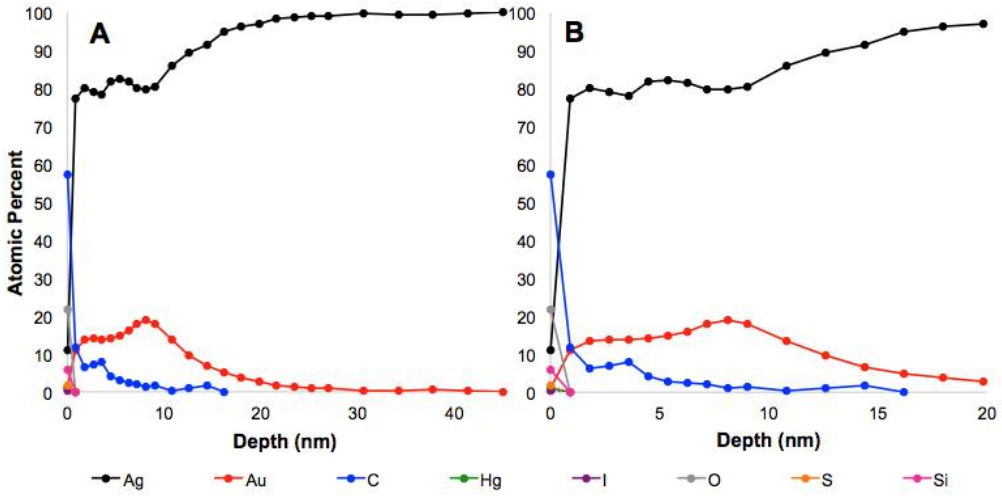

Fig 2. (A) XPS spectra of L1 -bright to a depth of 45nm and (B) rescaled to a depth of 20nm to highlight the near-surface oscillations of the elements of interest

677

After the removal of carbon on the sample surface, apparent maxima appear for Ag ($3d_{5/2,3/2}$), Au ($4f_{5/2,7/2}$), Hg ($4f_{5/2,7/2}$), Cl ($2p_{3/2,1/2}$) and I ($3d_{5/2,3/2}$) before the surface is sufficiently cleaned that the Ag substrate yield approaches 100%. Representative depth spectra for area L1 is shown in Fig 2 (L2 and L3 not shown). The maximum atomic percentages and associated depths for each element of interest are presented in table 1.

Table 1. Maximum atomic percent and the associated depth for each element of interest at three regions studied

Element	Area L1 - bright		Area L2 - medium		Area L3 - dark	
	Max. Atomic (%)	Depth (nm)	Max. Atomic (%)	Depth (nm)	Max. Atomic (%)	Depth (nm)
Silver (Ag)	100	45	100	41	100	34
Gold (Au)	19.0	8	17.5	7	16.3	11
Mercury (Hg)	0.9	< 2	0.3	< 2	0.1	< 2
Chlorine (Cl)	--	--	0.7	< 2	1.0	< 2
Iodine (I)	0.4	< 2	0.4	< 2	0.5	< 2

While there are distinct maxima in each of the Au depth profiles, the Au appears to persist to a depth of at least 45 nm. The simultaneous rise of the Ag and Au signal is consistent with the formation of an Au-Ag alloy, which remains relatively uniform within the first 12 nm. Mercury appears to be confined to the immediate surface and to be more abundant in the highlighted areas (L1) as seen in Fig 3, corresponding to the increased density of Ag-Hg image particles in these regions. Depth profiles for each element can be seen in Fig 3.

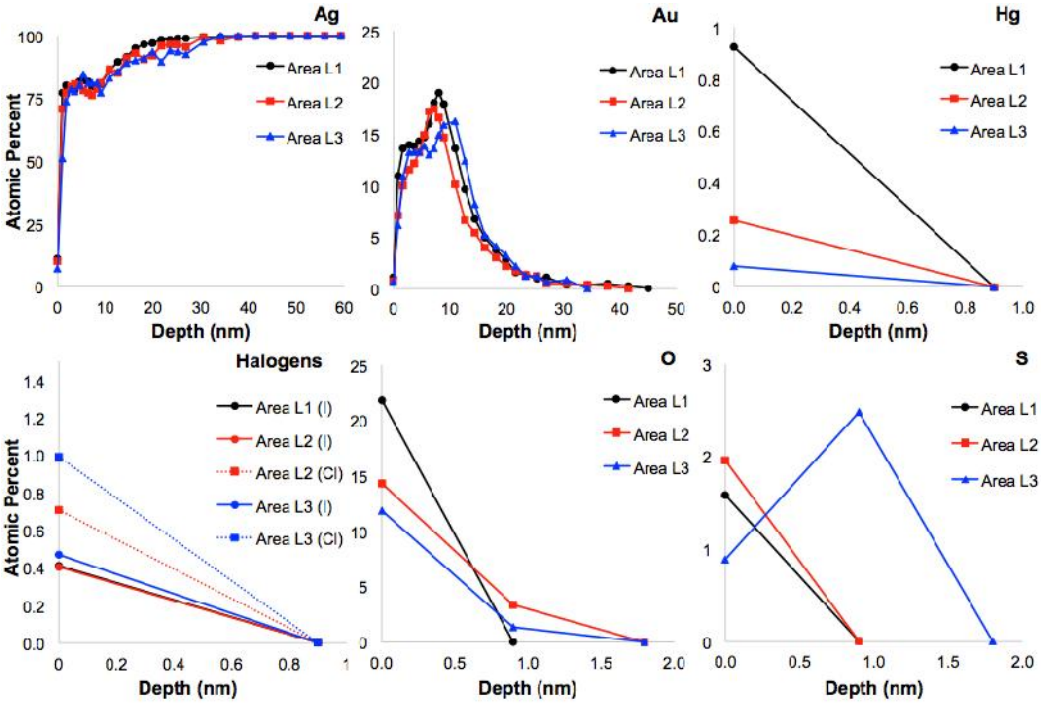

Fig 3. Depth scans for Ag, Au, Hg, I, Cl, O, and S at all regions studied (L1 - bright, L2 - medium, L3 - dark)

Oxygen, Hg, Cl, and I were present within the first 2 nm and were not detected after 30 minutes of etch time. Surface iodine is detected in all areas at low concentration and is possibly the result of incomplete removal of the original AgI. Chlorine was detected in area L2

(medium) and L3 (dark) but not in L1 (bright). Although this may be the result of incomplete removal as with iodine, AgCl may also be partly removed via photolysis.

The presence of S at the surface could be the remnants of the fixing thiosulfate solution or an environmental contaminant. Although the origin of Si is unclear, it may be due to the polishing process; the presented sample was polished with 3M abrasive papers and Nuvite polishing paste, or a thin silicone contaminant layer.

In (Fig 4), fine scans of Hg are shown above their respective SEM images. The observed Hg binding energies (BE) for regions L1-3 are shown in Table 2. The least amount of Hg was observed in area L3 and can be attributed to the lack of image particles, and consequently diminished surface area, in this region. Conversely, the greatest amount of Hg was observed in region L1, correlating to the highest density of image particles in this area. As L3 lies on the edge of the plate, a lower halogen and Hg concentration is expected; Ag and Au will be the primary elements present.

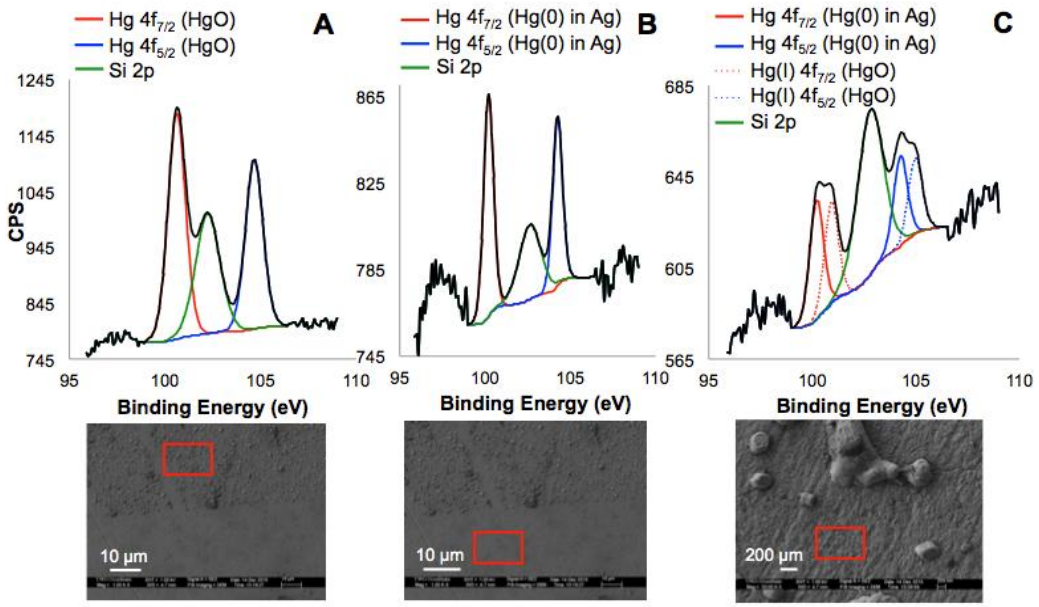

Fig 4. Hg fine scan on the daguerreotype test plate from the laboratory-based XPS source from (A) area L1 - bright, (B) area L2 - medium, and (C) area L3 - dark; SEM images shown below each spectrum with the area of interest shown with a red rectangle

Table 2. Binding energies for Hg $4f_{7/2}$ and $4f_{5/2}$ alongside proposed Hg sources

Area	$4f_{7/2}$ Peak Location (eV)	$4f_{5/2}$ Peak Location (eV)	Proposed Source(s)
L1 - bright	100.6	104.7	HgO
L2 - medium	100.2	104.3	Hg-Ag alloy
L3 - dark	100.2 100.9	104.3 100.5	~55% Ag-Hg alloy ~ 45% HgO

The most probable explanation for the excitation at 100.6eV is a Hg-Ag interaction with the possibility of HgO on the surface [12, 13]; this is supported by the noticeable broadening of the 4f7/2 peak. The fact that Hg(0) is not explicitly observed as a dominant peak is due to the presence of surface oxide, it supports the greatest density of oxide covered Ag-Hg image particles found in this region [14]. While their structural phase(s) is still unclear, Ag-Hg image

particles have been previously reported by Barger [3], Swan [15], and Ravines [2]. The formation of HgO may have occurred during the exposure of the plate to Hg vapour in the development step. From the depth profiles in Fig 3, O is present in regions L1-3. During the developing process, regions that were not exposed to light (i.e., midtone and shadow regions) still possess a halide layer over the Ag substrate, thus limiting and preventing the interaction the positively charged Hg droplets have with the Ag surface [16]. However, some interaction between Hg and Cl can be expected due to the number of lattice defects in the mixed Ag-halide layer [2]; for this reason, HgCl formation is possible in the shadow region, L3 [17]. As HgCl forms a white precipitate, this may be a contributing source, along with AgCl, to the white haze that is known to reduce visibility of the daguerreian image [18].

The fine scan spectra for Ag and Au (not shown) are similar to those reported by *K.S. Kim and N. Winograd* [19] and *L. Bzowski et al.* [20] and are consistent with the formation of an alloy in the near surface. This, along with the persistence of Au in the depth profiles (Fig 3) suggests that Au is present in an Au-Ag alloy and that the composition of the alloy remains uniform in the near surface volume. The laboratory-based Valence Band (VB) spectra were recorded from regions L1 and L2 only confirms this notion (not shown).

HE-XPS results

The HE-XPS survey spectra (Fig 5) were collected at 3.0keV and 8.0keV. Based on the density of pure Ag, the estimated analysis escape depth is 10nm and 20nm for 3.0keV and 8.0keV, respectively [21]. Characteristic core level peaks for metallic Ag (3d), Au (4f), and Hg (4f) were observed. It should be noted that the absorption cross-section and the photoionization cross-section drops by one order of magnitude going from 3keV to 8keV, fortunately the drop is comparable in both case so that we can make semi-quantitative comparison [22]. Comparison of the spectrum at 3.0keV to that at 8.0keV allows the surface and bulk element distribution to be distinguished non-destructively. The data clearly reveals the presence of Hg near the surface (inset of Fig. 5), in good accord with the depth profile results. A comparison of a bright region (S1) and a dark region (S2) with HE-XPS at 3.0keV reveals the presence of I, Cl, Au, S, Hg, and O along with the dominant Ag signal (Fig 6. 6).

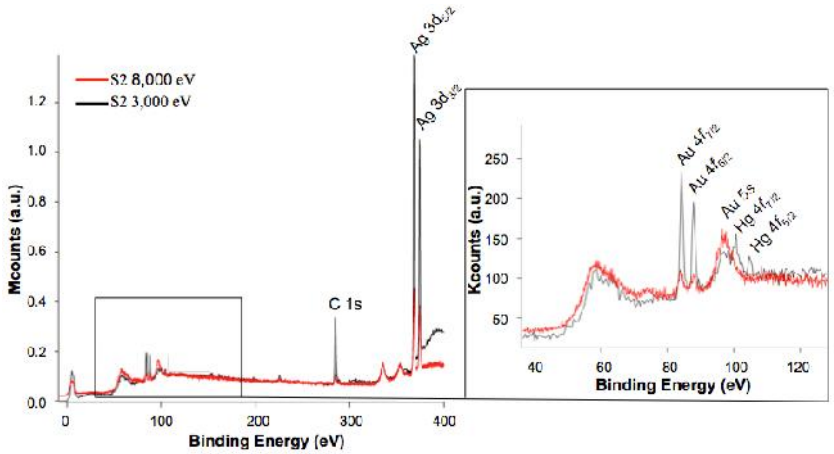

Fig 5. Comparison of two different incident energies at region S2 - dark: 3,000eV (surface) and 8,000eV (bulk)

A variation in the Au-Ag ratio (Table 3) indicates an increase in an Au concentration with depth; this is in part contributed by the increasing kinetic energy of the Au 4f electrons and the penetration depth of the photon through a homogeneous region of Au-Ag alloys. Table 3 shows that Au increases with depth. These results correspond to the Au depth profiles in Fig 3 as Au plateaus before reaching its max at 486, 378 and 540nm for regions L1-3, respectively.

Comparing the Au $4f_{7/2}$/Ag $3d_{5/2}$ ratio within the highlight and the midtone region at all three energies, an increase of ~47% and ~60% in the Au/Ag ratio for the highlight and midtone region, respectively, is observed with increasing depth. This slightly smaller degree of Au presence in the highlight region may suggest that the small particles constrain the diffusion process.

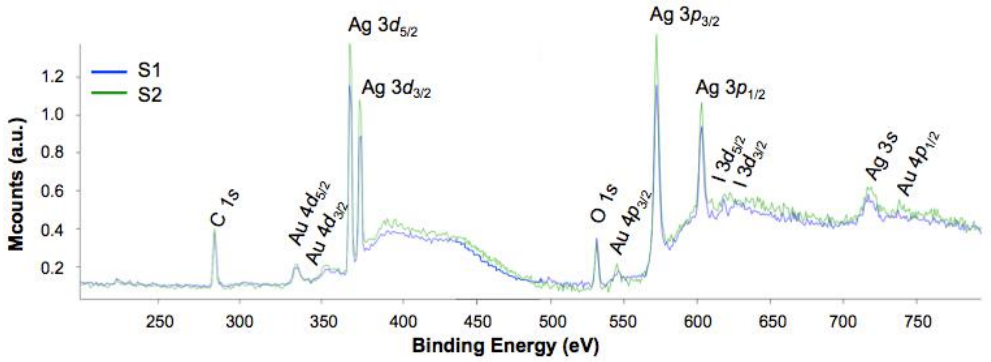

Fig 6. HE-XPS spectra comparing regions S1 (bright) and S2 (dark) of the daguerreotype test plate

Table 3. Ratio of Au $4f_{7/2}$/Ag $3d_{5/2}$ within a highlight region (S3) and a mid-tone region (S4) at all three energies: 1.4keV (shallow depth), 3keV (medium depth), and 8keV (deep depth)

	Lab XPS (1.4keV)	HE-XPS (3keV)	HE-XPS (8keV)
S3 - Bright	0.116	0.166	0.248
S4 - Medium	0.134	0.156	0.226

Fine spectra of Ag, Au, and the VB from the HE-XPS (3.0keV) to the lab XPS source (1.4867keV) were compared (not shown); the Ag and Au fine scans do not reveal any variations in binding energy noticeably away from metallic character.

The VB from the HE-XPS (Fig 7) shows Hg peaks at 8.2±0.2eV and 10.91±0.1eV, a spin-orbit doublet of the $5d_{3/2}$ and $5d_{5/2}$ orbitals, respectively [23]. The intensity of this feature is greatest in area S3 (bright) and weakest in S2 (dark) on the test plate. These doublet intensities correspond to a relative decrease and increase in the Au intensity for regions S3 (bright) and S2 (dark), respectively, consistent with formation of an Ag-Au alloy. The valence band shows that the Hg 5d band exhibits little hybridization with either Au or Ag, contradicting the understanding that the image particle is comprised of an Ag-Hg amalgam [15].

The VB is sensitive to the alloying of Ag-Au, which varies with depth in this sample. The Ag-Au alloy is confirmed by the apparent spin-orbit splitting:

$$\Delta_{obs} = \sqrt{\Delta_{so}^2 + \Delta_{5d}^2} \ ,$$

observed in the VB (Fig 7) [24]. The literature suggests that the d-band narrows as well as the apparent spin orbit splitting, going from pure Au to dilute Ag-Au can be observed in XPS [20]. The Au 5d bandwidth (Δ_{5d}) is very sensitive to the number of surrounding Au neighbor atoms and this band term decreases with the number of nearest neighbours [24].

Using the band term calculation method from *B.L. Henke et al.* [21], the band term was calculated for regions S1 – S4 as 1.842eV, 1.837eV, 1.842eV, and 1.952eV, respectively. Pure Au metal has an apparent 5d splitting of 2.72eV that reduces upon dilution into the Ag-Au form and, in some instances, can approach Au's atomic value of 1.52eV [20]. As the number of peripheral Au atoms decreases, the Δ_{5d} value decreases. Therefore, as S4 [medium] has the highest Δ_{5d} parameter the greatest amount of Au-Au interaction occurs in this region, indicating

681

a slightly Au-rich alloy compared to other regions. Correspondingly, the other regions have a smallest Δ_{5d} parameter but comparable among themselves, indicating uniformity.

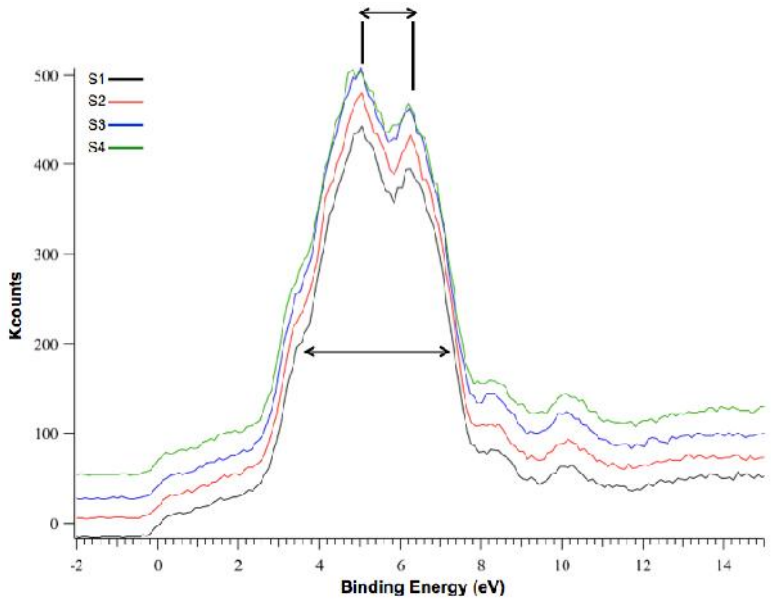

Fig 7. Valence band binding energies collected from daguerreotype test plate from HE-XPS: collected at an energy of 3,000eV for regions S1 - bright medium, S2 - dark, S3 - bright, and S4 - medium. The band width and apparent 5d spin-orbit splitting is shown

A simultaneous BE shift is observed in the peaks for both Au 4f and Ag 3d: a positive BE shift for Au with a negative BE shift for Ag. This further corroborates the alloying between Ag and Au. The intensity reduction of the S4 (medium) Au 4f peak indicates an increased degree of diffusion of Au into the Ag substrate, an expected characteristic of this particle bare region [20]: Ag-Au alloy forms in the bulk of the material. Similar characteristics of Ag-Au alloying are observed in the Ag 3d feature; the decrease of Ag 3d peak intensity of S4 (medium) relative to S3 (bright) is indicative of Au and Ag intermixing.

It should be noted that laboratory-based XPS ion ablation methods should only be used with caution on historic plates as it leads to visible surface alteration. However, no visible alteration was observed on the test plate resulting from of the HE-XPS. It merely takes advantage of the kinetic energy dependence of the escape depth of the electrons to sample different depths of interest. Localized heating from the X-ray beam and radiation damage would also induce chemical alteration, although no visible change was observed from this effect in this study. Therefore, HE-XPS is a viable method for the analysis of historic daguerreotypes; beam current and time under beam should be selected with care especially for non-metallic surfaces.

Conclusions

The use of both laboratory-based and HE-XPS sources enable the examination of varying depths within the daguerreian test plates. Both sources showed Hg to be present only within the first 1-2nm of the surface and to undergo possible alloying with Ag. This suggests that the Ag-Hg alloy is not as substantial as previously reported. Laboratory-based XPS also shows the possibility of HgCl in the shadow regions of the plate and may be the source for the white haze that previously has been attributed to AgCl; this may be the result of incomplete halide removal during the thiosulfate wash or from the gilding solution. Depth profiles from

XPS provided evidence of the formation of Au-Ag alloys. This was confirmed by HE-XPS Au $4f_{7/2}$/Ag $3d_{5/2}$ ratios at 3.0 and 8.0keV. The element distribution does not appear to have an effect more than the particle size and distribution. This work suggests the persistence of halides on the daguerreian surface and may impact their longevity and the conservation practices used in their preservation.

Acknowledgements

This research was supported by the National Science and Engineering Research Council of Canada, the Canadian Foundation for Innovation, Canada Research Chairs (TKS) and the Ontario Ministry of Innovation. Further support for interdisciplinary research was provided by The Dean's Office at The University of Western Ontario, Faculty of Science. Synchrotron experiments were performed at the Canadian Light Source, which is supported by NSERC, NRC, CIHR and the University of Saskatchewan. The Kratos Axis Ultra at Surface Science Western was supported by the Canadian Foundation for Innovation and the Ontario Research Fund.

References

[1] E. Da Silva, M. Robinson, C. Evans, A. Pejovic-Milic, D.V. Heyd, *Monitoring the photographic process, degradation and restoration of 21st century Daguerreotypes by wavelength-dispersive X-ray fluorescence spectrometry,* **Journal of Analytical Atomic Spectrometry, 25**(5)**,** 2010, pp. 654-661.

[2] P. Ravines, L. Li, R. McElroy, *An electron microscopy study of the image making process of the daguerreotype, the 19th century's first commercially viable photographic process,* **Journal of Imaging Science and Technology, 60**(3), 2016, Article Number: 030504.

[3] S.M. Barger, W.B. White, **The Daguerreotype: 19th Century and Modern Science, 1st ed.**, Published by Smithsonian Institution Press, John Hopkins University Press, Washington, DC, 1991, pp. 120-122, ISBN: 9780874743487.

[4] I. Motoyoshi, S. Nishida, L. Sharan, E.H. Adelson, *Images statistics and the perception of surface qualities,* **Nature, 447**(7141)**,** 2007, pp. 206-209.

[5] S.D. Humphrey, **American Hand Book of the Daguerreotype: Giving the Most Approved and Convenient Methods for Preparing the Chemicals, and the Combinations Used in the Art. Containing the Daguerreotype, Electrotype, and Various Other Processes Employed in Taking Heliographic Impression,** (fifth edition), S.D. Humphrey, New York, 1858.

[6] E.A. Marquis, Y. Chen, J. Kohanek, Y. Dong, S.A. Cenento, *Exposing the sub-surface of historical daguerreotypes and the effects of sulfur-induced corrosion*, **Corrosion Science, 94,** 2015, pp. 438-444.

[7] S.M. Barger, R. Messier, W.B. White, *Gilding and sealing daguerreotypes,* **Photographic Science and Engineering, 27**(4), 1983, pp. 141–146.

[8] W.C. Mallard, A.B. Gardner, R.F. Bass, L.M. Slifkin, *Self-diffusion in silver-gold solid solutions,* **Physical Review, 129**(2), 1963, pp. 617-625.

[9] M.C. Biesinger, C. Brown, J.R. Mycroft, R.D. Davidson, N.S. Mcintyre, *X-ray photoelectron spectroscopy studies of chromium compounds,* **Surface and Interface Analysis, 36**(12), 2004, pp. 1550–1563.

[10] Y.F. Hu, I. Coulthard, D. Chevrier, G. Wright, R. Igarashi, A. Sitnikov, B.W. Yates, E.L. Hallin, T.K. Sham, R. Reininger, *Preliminary Commissioning and Performance of the Soft X-ray Micro-characterization Beamline at the Canadian Light Source*, **The 10th International Conference on Synchrotron Radiation Instrumentation**, **Book**

683

Series: AIP Conference Proceedings, 27 September- 2 October 2009, **American Institute of Physics Conference Proceedings, 1234**(1)**,** 2010, pp. 343-346.

[11] *Igor Pro,* **WaveMetrics, Inc.,** (Wavemetrics, Lake Oswego, OR, USA), https://www.wavemetrics.com/products/igorpro/manual.htm. [Accessed 06.03.2016].

[12] A.V. Naumkin, A. Kraut-Vass, S.W. Gaarenstroom, C.J. Powell, *NIST X-ray Photoelectron Spectroscopy Database,* **NIST Standard Reference Database 20, Version 4.1**, http:/srdata.nist.gov/xps/ [accessed 09.30.2016].

[13] M. Uo, A. Berglund, J. Cardenas, L. Pohl, F. Wateri, M. Bergman, S. Sjoberb, *Surface analysis of dental amalgams by X-ray photoelectron spectroscopy and X-ray diffraction,* **Dental Materials, 19**(7), 2003, pp. 639-644.

[14] P. Ravines, L. Li, L. Chan, R. McElroy, **Nanoscience and Cultural Heritage**, (Editors: P. Dillmann, L. Bellot-Gurlet, I. Nenner) Atlantis Press: Chaville, France, 2016, p. 141.

[15] A. Swan, C.E. Fiori, and K.F.J. Heinrich, *Daguerreotypes: a study of the plates and the process,* **Scanning Electron Microscopy, 1,** 1979, pp. 411-423.

[16] I. Brodie, M. Thackray*, Photocharging of thin films of silver-iodide and its relevance to the Daguerre photographic process*, **Nature, 312**(5996)**,** 1984, pp. 744-746.

[17] G.T. Patterson, R. Passino, **Metals Speciation, Separations, and Recovery**, Vol. II, Lewis Publishers: Michigan, 1990, p. 55.

[18] H. Watts, M. Muir, M.M. Morley, **Watt's Dictionary of Chemistry**, Longmans, Green, and Co. and New York, 1892, pp. 213.

[19] K.S. Kim, N. Winograd, *X-ray photoelectron spectroscopic binding-energy shifts due to matrix in alloys and small supported metal particles*, **Chemical Physics Letters, 30**(1), 1975, pp. 91-95.

[20] A. Bzowski, M. Kuhn, T.K. Sham, K.H. Tan, *2-dimensional alloying of Au and Ag overlayer on Ru(001) - photoremission and thermal-desorption spectroscopy studies*, **Journal of Vacuum Science and Technology A: Vacuum Surfaces and Films, 12**(4), Part: 2, 1994, pp. 1790-1794.

[21] B.L. Henke, E.M. Gullikson, J.C. Davis, *X-Ray Interactions - Photoabsorption, Scattering, Transmission and Reflection at E = 50-30,000 eV, Z = 1-92,* **Atomic Data and Nuclear Data Tables, 54**(2), 1993, pp. 181-342.

[22] A.C. Thompson, D.T. Attwood, E.M. Gullikson, M.R. Howells, J.B. Kortright, A.L. Robinson, J.H. Underwood, K-J. Kim, J. Kirz, I. Lindau, P. Pianetta, H. Winick, G.P. Williams, J.H. Scofield, **X-ray Data Booklet** (second edition), Berkeley, California: Lawrence Berkeley National Laboratory, 2001.

[23] P.A. Dowben, Y.J. Kime, S. Varma, M. Onellion, J.L. Erskine, *Interaction of Hg overlayers with an Ag(100) surface,* **Physical Reviews B, 36**(5), 1987, pp. 2519-2529.

[24] T.K. Sham, *Nanoparticles and nanowires: synchrotron spectroscopy studies*, **International Journal of Nanotechnology, 5**(9-12), 2008, pp. 1194-1246.

Received: February 20, 2017
Accepted: November 25, 2017